The Fluid Dynamics of a Rocket Launch and Its Mathematical Description: Newton, Euler, Lagrange, Hamilton, and Poisson

How the classical formulations of mechanics organize fin design, launch stability, and apogee for small unguided rockets

Abstract

A model rocket leaving its launch rail at 20 m/s and coasting to apogee below 100 m/s occupies a narrow but instructive corner of fluid dynamics: incompressible flow at chord Reynolds numbers near 2×10^5, where skin friction, interference, and tip-vortex induced drag decide whether the vehicle reaches 190 m or 220 m on the same motor. This paper assembles the physics of that launch — drawn from a comparative review of fin-planform aerodynamics, a variational analysis of fin design, and an equal-area flight-experiment protocol — and expresses it in the five classical mathematical languages of mechanics. Newton's variable-mass equation, integrated numerically for a 62 g rocket on a B6-class motor, converts published planform drag coefficients (0.42 to 0.54) into a 17 m apogee spread. The Euler and Navier–Stokes field equations, with the pressure Poisson equation they imply, fix the flow regime and the drag budget. Lagrange's equations in the coordinates (h, θ) reduce launch stability to a damped oscillator whose stiffness is the static margin; the same Euler–Lagrange formalism, applied with a Lagrange multiplier to Prandtl's lifting-line functionals, yields the elliptical lift distribution as the unique minimum of induced drag, the theoretical root of the 25% drag reduction (6.37 N versus 8.50 N at 66 m/s) reported for elliptical fins in CFD validated by flight test. Hamilton's canonical equations recast the pitch dynamics in phase space, where aerodynamic damping appears as a monotonic drain on the Hamiltonian, and the Poisson bracket ties the fin set's rotational symmetry to conservation of roll angular momentum. The five formulations are not alternatives but one structure viewed from five angles, and each angle answers a design question the others leave implicit. A nozzle-flow analysis supplies the thrust term $F(t)$ that drives Newton's equation, and a Reynolds-number account of the boundary layer explains why the vehicle's skin friction, and on occasion its total drag, can rise or fall sharply as the flow trips from laminar to turbulent.

Keywords: *rocket launch; fin planform; induced drag; Euler equations; Navier–Stokes equations; Reynolds number; boundary layer; drag crisis; de Laval nozzle; Laplace's equation; Lagrangian mechanics; Hamiltonian mechanics; Poisson bracket; static margin; lifting-line theory*

1. Introduction

Ask why a rocket flies straight and you will get an answer about fins. Ask why the fins are shaped the way they are, and the answer runs deeper than aerodynamic folklore: it runs through the whole architecture of classical mechanics. The restoring moment that straightens a gust-disturbed rocket is a term in Lagrange's equations. The elliptical lift distribution that minimizes fin drag is the solution of an Euler–Lagrange equation with a Lagrange multiplier. The roll spin that a badly aligned fin set acquires is a broken symmetry, and its absence on a well-built rocket is a conservation law expressible as a vanishing Poisson bracket. None of this is decoration. Each formulation answers a question the others leave implicit, and a designer who can move between them holds a sharper set of tools than one who memorizes rules of thumb.

This paper builds that argument on three specific sources. A comparative review of fin-planform aerodynamics supplies the empirical record: CFD, wind-tunnel, and flight-test comparisons of rectangular, trapezoidal, clipped delta, swept, and elliptical fins, including a flight-validated 25% drag reduction for an elliptical-fin configuration [4] and simulation campaigns that repeatedly place the trapezoid at the top of the apogee rankings [5, 7]. A variational analysis of fin design supplies the theory, deriving the planform rankings and the stability rules from lifting-line theory and analytical mechanics rather than asserting them. And an equal-area flight protocol for the same four planforms, flown on identical airframes and analyzed by one-way ANOVA over repeated flights, supplies the experimental counterpart [10]. The apogee figures this paper works with, roughly 188 to 217 m, are not measurements from that protocol but predictions the sections below derive from published planform drag coefficients. What the three sources share, and what this paper makes explicit, is mathematics. Sections 2 and 3 set out the fluid mechanics of the launch in Eulerian field form. Section 4 works through the vehicle's motion four ways — Newton, Lagrange, Hamilton, Poisson — using the pitch dynamics of a launching rocket as the running example. Section 5 returns to the fin and shows that its optimal shape is itself a variational result, then confronts theory with the published measurements. Section 6 completes the fluid picture opened in Section 2 by working out the thrust the motor supplies and the drag budget the airframe pays, and Section 7 returns to the Reynolds number of Section 3 to derive the boundary layer, the skin friction, and the drag crisis it can trigger. Section 8 outlines how a student team can test the whole structure for about US$120.

2. Describing the Flow: Lagrange's Particles and Euler's Fields

Fluid mechanics offers two complete descriptions of the same motion, and both carry the names that recur throughout this paper. The Lagrangian description follows individual fluid parcels along their trajectories, as one follows the smoke particle that traces a tip vortex. The Eulerian description fixes attention on points in space and records the velocity field u(x, t) passing through them, the natural frame for a fin, which sits still in the body frame while air streams past. The two are linked by the material derivative,

$$Du/Dt = \partial u/\partial t + (u \cdot \nabla)u \qquad (1)$$

which is the acceleration of a Lagrangian parcel written in Eulerian variables. The convective term $(u \cdot \nabla)u$ is nonlinear, and nearly everything difficult in fluid dynamics — turbulence included — descends from it.

For the speeds of a model rocket launch, below 100 m/s and hence below Mach 0.3, the flow is incompressible to within about 4% density variation, so mass conservation reduces to

$$\nabla \cdot u = 0 \qquad (2)$$

Momentum conservation for an ideal (inviscid) fluid gives the Euler equations,

$$\rho\, Du/Dt = -\nabla p + \rho g \qquad (3)$$

and restoring viscosity gives the Navier–Stokes equations,

$$\rho\, Du/Dt = -\nabla p + \mu \nabla^2 u + \rho g \qquad (4)$$

Equation (4) with (2) is four equations for four unknowns (u, p), but the pressure has no evolution equation of its own. Taking the divergence of (4) and applying (2) eliminates the time derivative and leaves

$$\nabla^2 p = -\rho\, \nabla \cdot [(u \cdot \nabla)u] \qquad (5)$$

a Poisson equation: the pressure field at any instant is determined by the velocity field at that same instant, as if by electrostatics with the convective term as source. This is Poisson's first appearance in the paper. His second, the Poisson bracket of Hamiltonian mechanics, arrives in Section 4.4, and the coincidence of names is worth savoring: the same mathematician supplied both the equation that fixes the pressure on a fin and the algebraic structure that organizes the rocket's conservation laws.

3. The Flow a Launching Rocket Actually Sees

Numbers first. A fin of root chord $c \approx 6$ cm on a rocket passing 60 m/s operates at a chord Reynolds number

$$Re\_c = vc/\nu \approx (60)(0.06)/(1.5 \times 10^{-5}) \approx 2.4 \times 10^{5} \qquad (6)$$

This is the transitional regime: inertial forces dominate, yet a smooth surface can hold the boundary layer laminar over much of the chord. The Blasius flat-plate result gives laminar skin friction roughly half the turbulent value at this Reynolds number, which is why sealing and polishing balsa fins is an aerodynamic act, not a cosmetic one. Just off the launch rod the story is worse in two ways at once: v is several times smaller, so Re drops and the fins lose lift effectiveness exactly when the rocket has too little airspeed for its fins to correct a crosswind. Every launch-behavior observation in the experimental protocol [10] traces back to this low-speed window.

The drag of the fin set then decomposes into four parts, and the decomposition organizes everything a designer can do. Skin friction scales with wetted area and surface finish; it is paid at all times. Profile drag comes from the cross-section — a square-edged fin trips the boundary layer, and edge rounding alone can shift the drag coefficient by more than the choice of planform [8]. Interference drag arises where the fin root meets the body tube and two boundary layers merge; a small fillet of adhesive suppresses much of it. Induced drag is different in kind: it appears only when the fins generate lift, which is to say whenever they are doing their stabilizing job at nonzero angle of attack, and it is governed almost entirely by planform shape. Section 5 shows why. Above roughly Mach 0.8 a fifth term, wave drag, enters and reverses several of these rankings — clipped delta and swept planforms, mediocre at subsonic speed, become the lowest-drag options beyond Mach 1.5 because their swept leading edges stay behind the Mach cone [6]. The rockets considered here never get there; the point matters only as a warning against exporting subsonic conclusions to faster vehicles. Section 7 returns to the chord Reynolds number of Eq. (6) and derives, in full, the boundary layer it sets and the skin-friction and separation behavior that follow from it.

4. The Vehicle in Four Mathematical Languages

4.1 Newton: the variable-mass equation and what drag costs

Newton's second law for a rocket must account for the mass it throws away. With thrust $F = \dot{m}\_e\, v\_e$ (exhaust mass flow times exhaust velocity, derived from nozzle flow in Section 6), the vertical equation of motion is

$$m(t)\, dv/dt = F(t) - m(t)g - ½\, \rho\, v^2\, C\_D\, A\_ref \qquad (7)$$

and in vacuum, integrated over a burn, it yields Tsiolkovsky's relation

$$\Delta v = v\_e \ln(m_0/m\_f) \qquad (8)$$

For a model rocket the drag term rules. Because drag grows as v^2, it is most expensive near burnout velocity, and small differences in C_D compound over the coast. Figure 1 integrates Eq. (7) numerically for a 62 g rocket on a B6-class motor (5.8 N average thrust, 0.86 s burn) using the drag coefficients the planform literature assigns to the four fin shapes of the flight protocol: 0.42, 0.44, 0.48, and 0.54. The integration alone — no aerodynamic subtlety beyond a single C_D per vehicle — spreads the apogees from 191 m to 208 m. A literature-scaled estimate that resolves the fins in more detail spreads them slightly wider, to roughly 188 to 217 m. Either way the planform effect is two to three times the expected flight-to-flight scatter of 7–10 m, which is what makes it measurable by a school team.

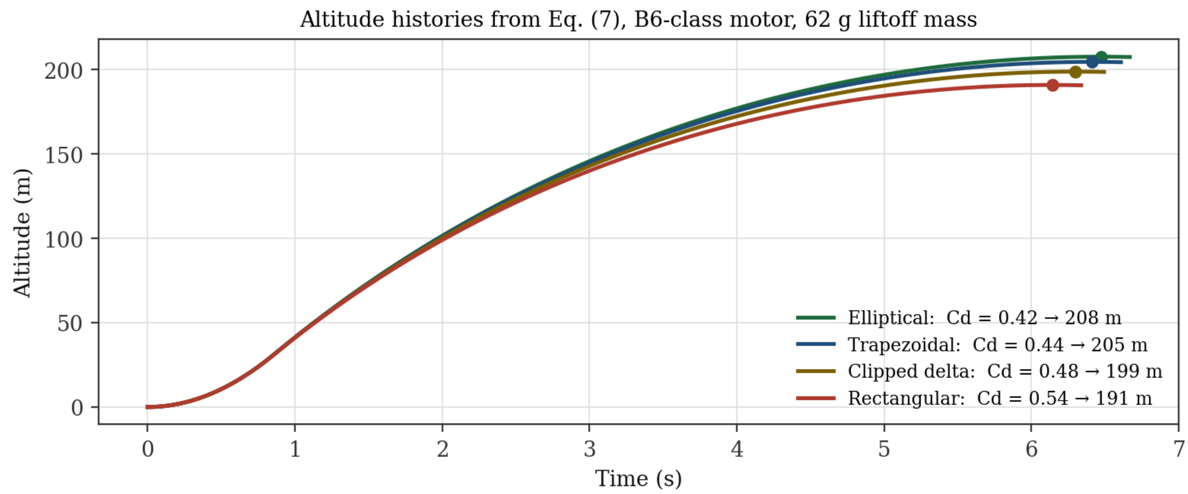

Figure 1. Altitude histories from numerical integration of Eq. (7) for a 62 g rocket on a B6-class motor, using the planform drag coefficients from the reviewed literature. The Cd spread of 0.42–0.54 becomes a 17 m apogee spread.

What Newton's formulation does not explain is why C_D differs between planforms of identical area, or what "statically stable" means in dynamical terms. Those answers need generalized coordinates.

4.2 Lagrange: the pitch oscillator hiding in the stability rule

Lagrangian mechanics replaces forces with energies. For planar flight two generalized coordinates suffice: altitude h and pitch angle θ between body axis and velocity vector. Aerodynamic forces dissipate energy, so Hamilton's principle extends to the Lagrange–d'Alembert form, with non-conservative effects entering as generalized forces Q_i:

$$\frac{d}{dt}\left(\frac{\partial L}{\partial \dot{q}_i}\right) - \frac{\partial L}{\partial q_i} = Q_i \qquad (9)$$

$$L = T - V = \tfrac{1}{2}\, m(t)\, \dot{h}^2 + \tfrac{1}{2}\, I(t)\, \dot{\theta}^2 - m(t)\, g\, h \qquad (10)$$

The h-equation reproduces Eq. (7). The θ-equation is where the fins live. A rocket pitched to small θ generates a fin normal force $\tfrac{1}{2}\rho v^2 S_f C_{N\alpha}\theta$ acting at the center of pressure, a lever arm $\Delta X = x_{CP} - x_{CG}$ behind the center of gravity:

$$Q_\theta \approx -\left[\tfrac{1}{2}\rho v^2 S_f C_{N\alpha} \Delta X\right]\theta - C_\theta \dot{\theta} \qquad (11)$$

so that the linearized pitch dynamics form a damped harmonic oscillator,

$$I\ddot{\theta} + C_\theta \dot{\theta} + \left[\tfrac{1}{2}\rho v^2 S_f C_{N\alpha} \Delta X\right]\theta = M_{gust}(t) \qquad (12)$$

Every rule of thumb in model rocketry is a statement about the coefficients of Eq. (12). The stiffness is proportional to the static margin ΔX: put the CP ahead of the CG and the stiffness goes negative — the "restoring" moment diverges and the rocket tumbles. Raise the margin past about two calibers and the natural frequency $\omega_n = \sqrt{\tfrac{1}{2}\rho v^2 S_f C_{N\alpha} \Delta X / I}$ grows so large that the rocket snaps its nose into any crosswind, trading altitude for alignment; this is weathercocking, and it is why the flight protocol treats the clipped delta's 2.1 calibers of margin as a liability in wind rather than a virtue [3, 10]. The damping C_θ is supplied mostly by the fins themselves, growing with span and area — which also grow drag, a tension resolved only by the optimization of Section 5. And because the stiffness carries a factor v^2, stability is weakest just off the rod, which is the dynamical restatement of the Reynolds argument of Section 3. Figure 2 shows the three regimes.

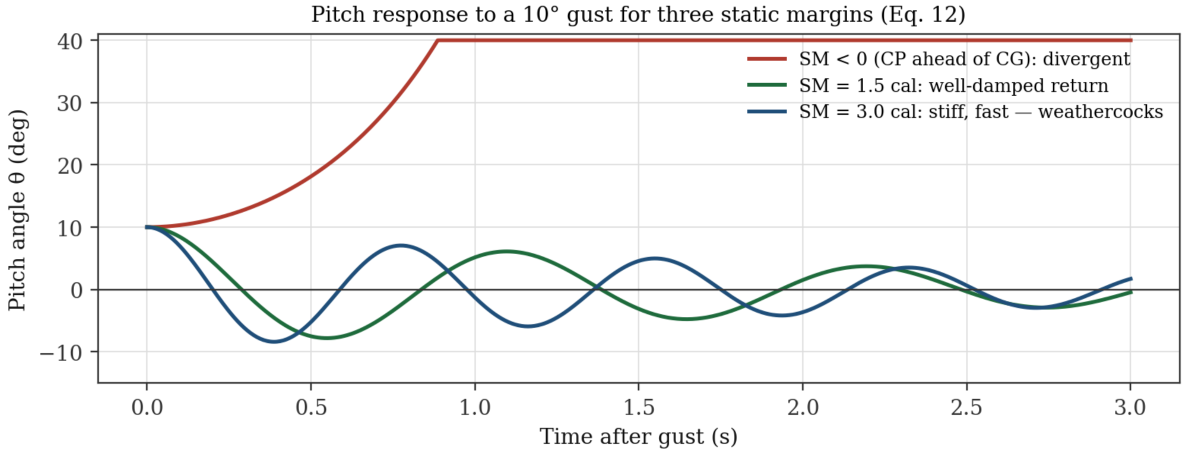

Figure 2. Pitch response to a 10° gust from Eq. (12). Negative margin diverges; 1.5 calibers absorbs the gust in a damped oscillation; 3 calibers responds stiffly and fast — the over-stable rocket that weathercocks into wind.

One further Lagrangian result deserves its place. A fin set of three or four identical fins spaced equally around the tube leaves L invariant under the corresponding rotations, and Noether's theorem converts that symmetry into conservation of roll angular momentum: a fin can built with perfect alignment, starting from zero spin, stays at zero spin. Misaligned fins break the symmetry, and the broken symmetry shows up as roll spin, coning, and a corkscrewed trajectory. Aligning fins with a jig is not craftsmanship for its own sake; it is the enforcement of a conservation law.

4.3 Hamilton: the same oscillator in phase space

The Hamiltonian formulation trades $\dot{\theta}$ for the conjugate momentum and turns one second-order equation into two first-order ones. Applying the Legendre transform to the pitch degree of freedom,

$$p = \partial L/\partial\theta = I\,\theta, \quad H(\theta, p) = p^2/2I + ½\,k\,\theta^2, \quad k = ½\,\rho\,v^2\,S\_f\,C\_N\alpha\,\Delta X \qquad (13)$$

$$\theta = \partial H/\partial p, \quad \dot{p} = -\partial H/\partial\theta + Q\_\theta \qquad (14)$$

For the conservative part, H is the pitch energy and is constant along trajectories: the motion runs along the elliptical energy contours of the (θ, p) plane. Aerodynamic damping enters through Q_θ and does exactly one thing to this picture:

$$dH/dt = -C\_\theta\,\theta^2 \le 0 \qquad (15)$$

The Hamiltonian can only decrease. A gust deposits the rocket on a high-energy contour; drag then walks it monotonically down the contour ladder until it rests at the trim point. Figure 3 shows the spiral. The value of this reformulation is not computational — Eq. (12) was already solvable — but diagnostic. Stability becomes geometry: a stable rocket has closed energy contours around trim and a dissipation term that cannot raise H; an unstable one ($k < 0$) has saddle-shaped contours from which no amount of damping can rescue it. The phase portrait also makes the launch-rod argument vivid: since $k \propto v^2$, the contours flatten as $v \to 0$, and near the rod the "well" holding the rocket upright is shallow.

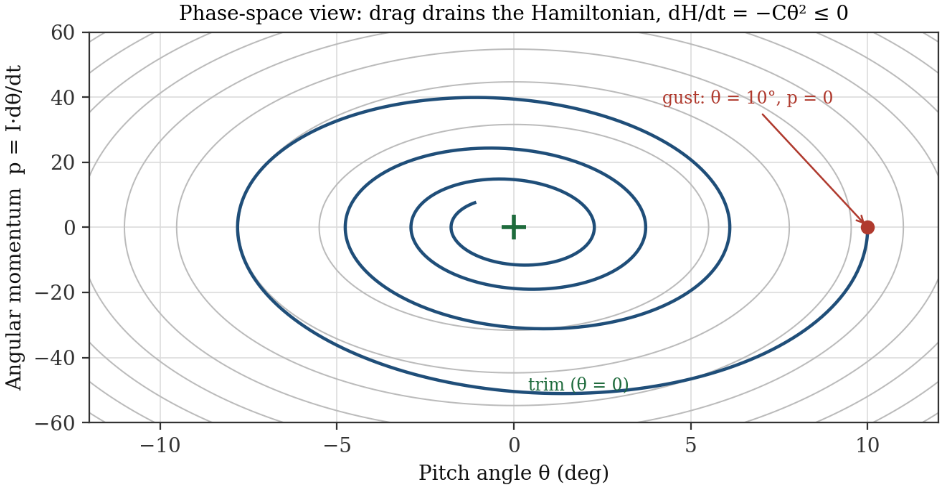

Figure 3. The pitch dynamics of Figure 2 (SM = 1.5 cal) in phase space. Grey curves are contours of the Hamiltonian; the damped trajectory crosses them inward, since Eq. (15) forbids H from rising, and spirals to trim.

4.4 Poisson: brackets, conservation, and the algebra of what stays fixed

Hamilton's equations (14) compress into a single algebraic statement. Define the Poisson bracket of two phase-space functions,

$$\{F, G\} = (\partial F/\partial\theta)(\partial G/\partial p) - (\partial F/\partial p)(\partial G/\partial\theta) \qquad (16)$$

Then any observable F evolves as

$$dF/dt = \{F, H\} + \partial F/\partial t \qquad (17)$$

and the canonical pair itself satisfies $\{\theta, p\} = 1$. The bracket is where conservation laws become checkable by differentiation: F is conserved exactly when its bracket with the Hamiltonian vanishes. Noether's roll result of Section 4.2 reads, in this language, $\{L_{roll}, H\} = 0$ for a fin can whose Hamiltonian is invariant under the fin-spacing rotations — one line, no integration of trajectories required. For the launching rocket the bracket formalism is admittedly heavier machinery than the problem strictly needs; its payoff is conceptual economy. Newton gives the trajectory, Lagrange the equations from energies, Hamilton the geometry of energy flow, and Poisson the algebra of invariants — and all four are derivable from each other. A student who has watched the static margin appear as a force lever (Newton), an oscillator stiffness (Lagrange), a contour shape (Hamilton), and a bracket relation (Poisson) has seen classical mechanics whole, on a vehicle that costs twelve dollars.

5. The Fin as a Variational Problem, and What the Data Say

5.1 The Euler–Lagrange equation inside the planform question

Why should fin shape — not just fin area — control induced drag? A lifting fin carries a bound circulation $\Gamma(y)$ along its span, and by Kelvin's theorem that circulation cannot end at the tip; it is shed as a trailing vortex whose kinetic energy is the induced drag. Prandtl's lifting-line theory writes both lift and induced drag as functionals of the circulation distribution:

$$L[\Gamma] = \rho V \int \Gamma(y)\, dy, \quad D_i[\Gamma] = \rho \int \Gamma(y)\, w(y)\, dy \qquad (18)$$

with $w(y)$ the downwash of the trailing sheet. The design question — which $\Gamma(y)$ minimizes D_i at fixed lift L_0? — is the calculus of variations with a constraint, and the machinery is the same one that produced Eq. (9). Introducing a multiplier λ and demanding stationarity,

$$\delta/\delta\Gamma \{ D_i[\Gamma] - \lambda(L[\Gamma] - L_0) \} = 0 \implies w(y) = constant \qquad (19)$$

Uniform downwash across the span, and the unique distribution achieving it is the ellipse, $\Gamma(y) = \Gamma_0\sqrt{(1 - (y/s)^2)}$. The result propagates into the induced-drag coefficient through the span-efficiency factor e in $C_{Di} = C_L^2/(\pi e AR)$: the elliptical planform realizes e = 1 exactly, a trapezoid of taper ratio near 0.4–0.5 reaches e ≈ 0.98 with straight, buildable edges, and the rectangular fin, hauling full chord out to the tip, falls to e ≈ 0.85, an 18% induced-drag penalty carried on every stabilizing correction the fins make (Figure 4). Lagrange thus appears twice in this paper, and not by coincidence: his equations govern how the rocket moves, and his multipliers govern how its fin should be shaped. Both are stationarity conditions on a functional. Recognizing them as the same idea is, we think, the conceptual heart of the subject.

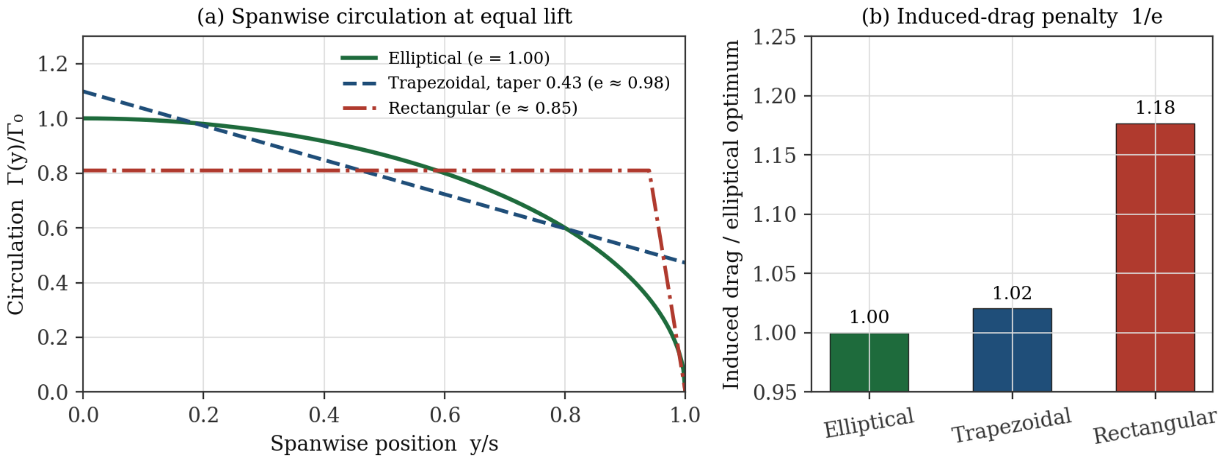

Figure 4. (a) Spanwise circulation at equal lift for three planforms; the ellipse is the solution of the constrained variational problem, Eq. (19). (b) The resulting induced-drag penalty relative to the elliptical optimum.

5.2 The empirical record

Theory this clean deserves suspicion, so it is worth stating how well the measurements cooperate. The flight-validated CFD study of twelve configurations found the elliptical-fin, ogive-nose vehicle at 6.37 N of drag at 66 m/s against 8.50 N for the unoptimized baseline — the 25% reduction quoted in every subsequent comparison — with the clipped triangular fins taking the largest static margin at slightly higher drag [4]. Simulation campaigns that score apogee rather than raw drag place the trapezoid first: 2,639 m for an ogive-plus-trapezoid sounding rocket across nine combinations [5], and greatest stability, highest altitude, and lowest C_D in a three-planform flight-plus-simulation comparison significant at $p < 0.0001$ [7]. A response-surface study adds the sizing caveat: span and root chord dominate both apogee and margin across all planforms, so shape selection cannot be divorced from sizing [3]. Figure 5 and Table 1 collect the numbers. The consistent picture is that the ellipse wins the physics and the trapezoid wins the engineering: its near-elliptical loading (e ≈ 0.98) costs almost nothing aerodynamically, and its straight edges accept the airfoiling that matters as much as planform [8].

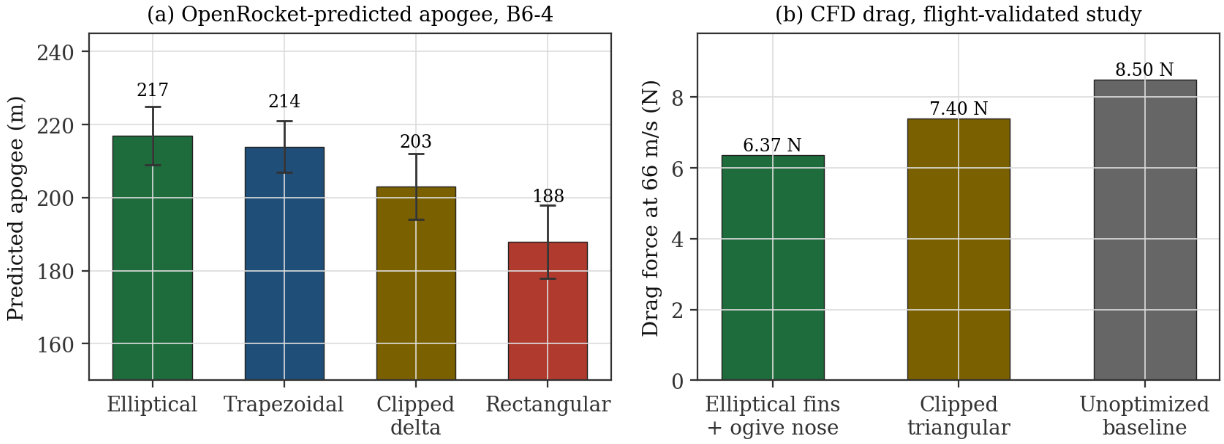

Figure 5. (a) Predicted apogee by planform for the equal-area flight protocol (OpenRocket, B6-4, error bars = expected SD). (b) Flight-validated CFD drag at 66 m/s: elliptical fins with an ogive nose cut drag 25% relative to the baseline.

Table 1. The four equal-area planforms of the flight protocol and their predicted performance (25 cm² per fin, 3 mm balsa, B6-4 motor, 62 g liftoff mass).

Planform	Root/tip chord (cm)	Predicted apogee (m)	Predicted Cd	Static margin (cal)	Span efficiency e
Elliptical	6.3 / 0	217 ± 8	0.42	1.3	1.00
Trapezoidal	7.0 / 3.0	214 ± 7	0.44	1.6	≈ 0.98
Clipped delta	8.0 / 2.0	203 ± 9	0.48	2.1	≈ 0.95
Rectangular	5.0 / 5.0	188 ± 10	0.54	1.4	≈ 0.85

5.3 Design as constrained optimization

Sections 4 and 5.1 leave fin design in the form of a well-posed problem: maximize the apogee functional over the design vector x (planform family, area, span, taper, sweep, thickness, edge profile), subject to $1 \leq SM(x) \leq 2$ calibers, flutter clearance, and manufacturability. The Lagrange-multiplier structure of Eq. (19) reappears at the design level, and it carries the single most useful insight the mathematics has to offer: the unconstrained optimum is a finless rocket, which is unstable, so the true optimum always sits on the stability constraint boundary. Optimal fin design is the art of buying exactly enough stability at minimum drag price: the smallest, smoothest, most efficiently loaded surface that still delivers its calibers of margin. In practice the search runs in three layers of increasing cost: Barrowman and lifting-line sensitivity analysis on paper, response-surface sweeps in OpenRocket, and randomized flight experiment as the final arbiter.

6. The Navier–Stokes Equations: Nozzle Flow, Thrust, and the Drag Budget

A rocket is two fluid-dynamics problems joined by a rigid airframe: the compressible flow of combustion gas that produces thrust, and the flow of atmosphere over the body that produces drag. Both obey the Navier–Stokes momentum equation, Eq. (4); the distinction between them is only which terms in that equation matter most. Inside the engine, pressure gradients and convective acceleration dominate, and the flow is well approximated as inviscid and compressible. Outside the engine, at the speeds of Section 3, the flow is nearly incompressible and the viscous term sets the friction budget that Section 7 takes up on its own.

6.1 The de Laval nozzle and the origin of thrust

Combustion gas leaves the chamber through a converging-diverging (de Laval) nozzle. It accelerates through the converging section, reaches sonic speed at the throat where the flow chokes, and continues to supersonic speed in the diverging section as its pressure falls; the process is closely isentropic. Applying the integral form of momentum conservation, the same physics as Eq. (4), to a control volume around the engine gives the thrust:

$$F = \dot{m}\, v\_e + (p\_e - p\_a)\, A\_e \qquad (20)$$

The first term, momentum thrust, is the rate at which momentum leaves the nozzle. The second, pressure thrust, is the imbalance between the exit pressure p_e and the ambient pressure p_a acting over the exit area A_e. A nozzle is optimally expanded when p_e = p_a; because p_a falls toward zero with altitude, a fixed engine gains thrust as the rocket climbs, and this pressure term alone is why a first-stage nozzle and a vacuum-optimized nozzle are cut to different expansion ratios [18].

The thrust F(t) that entered Newton's equation of motion in Section 4.1, Eq. (7), is Eq. (20) evaluated at the vehicle's current altitude. Writing the force balance along a general flight-path angle θ from vertical,

$$m\, dv/dt = F\_thrust - D - m\, g \cos\theta \qquad (21)$$

recovers Eq. (7) at θ = 0. Everything in Section 4, the pitch oscillator, the phase portrait, the Poisson bracket, sits beneath this scalar equation along the flight path; what turns a scalar drag D into a stabilizing or destabilizing moment is precisely the θ-equation buried in Eq. (9).

6.2 The drag budget

Drag itself is not one effect but several, each traceable to a specific term or boundary condition in the Navier–Stokes equations (Table 2). Skin-friction drag is the direct consequence of the viscous term $\mu\nabla^2 u$ evaluated at the wall, and Section 7 works it out term by term. Form (pressure) drag comes from the fore-aft imbalance in the pressure field, the same field fixed instant-by-instant by the Poisson equation, Eq. (5), and it grows sharply once the boundary layer separates. Interference drag, introduced in Section 3, is a local instance of the same pressure-imbalance mechanism where two boundary layers merge at the fin root. Induced drag is the subject of Section 5, and follows from the trailing-vortex functional of Eq. (18). Base drag is the low-pressure separated wake behind a blunt tail, with no laminar analogue. Wave drag appears only once the local Mach number exceeds unity somewhere on the body and is negligible for the sub-100-m/s launches this paper treats, though Section 3 already flagged it as a caveat for faster vehicles.

Table 2. Components of total drag and their origin in the Navier–Stokes equations.

Component	Governing term or mechanism	Physical origin
Skin friction	viscous term $\mu\nabla^2 u$; wall shear τ_w (Eq. 25)	boundary-layer friction, paid at all times (Sec. 7)
Form (pressure)	pressure field of the Poisson equation (Eq. 5); separation	fore-aft pressure imbalance, worsened by early separation
Interference	merging boundary layers at the fin-body junction	two boundary layers combining near the root (Sec. 3)
Induced	trailing-vortex functional (Eq. 18)	lift-dependent, governed by planform shape (Sec. 5)
Base	low-pressure separated wake behind a blunt tail	wake effect with no laminar analogue
Wave	shock formation above $M \approx 0.8$–1	compressibility; negligible below 100 m/s (Sec. 3)

6.3 The Laplace limit of the pressure Poisson equation

The Poisson equation of Section 2, Eq. (5), has a companion worth naming explicitly, since it is the second equation the paper's title omits but its physics requires. Far from the body, where the flow can be treated as irrotational, the velocity is the gradient of a scalar potential, $u = \nabla\varphi$, and the convective source term on the right of Eq. (5) vanishes identically. Continuity, Eq. (2), then reduces to Laplace's equation:

$$\nabla^2\varphi = 0 \qquad (22)$$

the same equation that governs electrostatic potential and steady heat conduction. Laplace's equation is the source-free limit of Poisson's (the same pairing, one mathematician, that Section 2 already flagged), and where Eq. (5) needs the whole velocity field to build the pressure field, Eq. (22) needs only boundary conditions on the body's surface, with the pressure following afterward from Bernoulli's equation rather than from an elliptic solve with a source term. Potential-flow panel methods, the fastest first-pass tool for estimating a rocket's pressure distribution before committing to a full CFD run, are built on exactly this simplification: solve Laplace's equation for the outer, irrotational flow, then patch the thin viscous boundary layer of Section 7 onto the surface where the no-slip condition actually lives.

6.4 Max-Q

One instant in the ascent deserves separate mention because it sizes the structure rather than the trajectory. Dynamic pressure,

$$q = ½ \rho v^2 \qquad (23)$$

is the product of a density that falls roughly exponentially with altitude and a speed that rises through the burn; the two trends cross at an intermediate altitude, producing a single maximum, Max-Q, that marks the greatest aerodynamic load the airframe and fins must survive in flight. A fin sized only against the C_D comparisons of Section 5, without a flutter and bending check at Max-Q, is sized for the wrong number.

7. The Reynolds Number: Boundary Layers and the Drag Crisis

Section 3 introduced the chord Reynolds number of a fin, Eq. (6), and asserted that it fixes the flow regime. This section makes that claim precise. The Reynolds number,

$$Re = \rho UL/\mu = UL/\nu \qquad (24)$$

compares the inertial term $\rho(u\cdot\nabla)u$ of Eq. (4) to the viscous term $\mu\nabla^2 u$. At the fin-chord values of Section 3, $Re \approx 2\times10^5$, both terms matter and the boundary layer sits in the transitional regime, where surface finish decides whether it stays laminar. Over the vehicle as a whole, at body-length scale, Re climbs to 10^7–10^8: inertia overwhelms viscosity almost everywhere, and friction is confined to a thin layer against the skin [17].

7.1 The boundary layer and wall shear

Within that thin layer the velocity rises from zero at the wall, the no-slip condition, to the free-stream value over a thickness δ, and the friction the vehicle feels is set entirely by the velocity gradient at the wall:

$$\tau\_w = \mu\ (\partial u/\partial y)\ \text{at}\ y = 0 \qquad (25)$$

For a laminar layer the Blasius solution gives

$$\delta/x = 5.0/\sqrt{Re\_x}\,,\quad C\_f{,}x = 0.664/\sqrt{Re\_x} \qquad (26)$$

while a turbulent layer, which thickens faster and carries a fuller velocity profile because its eddies mix high-momentum fluid down toward the wall, follows the empirical correlations

$$\delta/x \approx 0.37/Re\_x\text{^}0.2\,,\quad C\_f \approx 0.074/Re\_L\text{^}0.2 \qquad (27)$$

At the same Reynolds number the turbulent layer produces more skin-friction drag, not less, because its steeper near-wall gradient raises τ_w in Eq. (25). The resulting force, summed over the wetted area,

$$D\_f = ½\,\rho\,U^2\,C\_f\,A\_wetted \qquad (28)$$

is the skin-friction term of the drag budget in Table 2, and it is why sealing and polishing balsa fins, mentioned already in Section 3, is an aerodynamic act rather than a cosmetic one: a smoother surface delays the transition between Eq. (26) and Eq. (27) as long as possible.

7.2 Separation and the drag crisis

Friction reshapes more than the surface stress. A laminar layer carries little momentum near the wall and separates early when it meets a rising pressure gradient, opening a wide low-pressure wake and a large form-drag penalty. A turbulent layer, carrying more near-wall momentum, resists that adverse pressure gradient and stays attached longer, closing the wake even though its own surface friction is higher. The net result, the drag crisis, is that total drag can fall sharply as the Reynolds number crosses the transition value, because the reduction in wake (form) drag outweighs the increase in skin friction. For a rocket this same mechanism governs the size of the base-drag wake behind a blunt tail, and it is a second, independent reason, alongside the profile-drag argument of Section 3, that a rounded, transition-tripping edge can outperform a nominally smoother one over part of the flight envelope.

7.3 The Reynolds number over the ascent

The Reynolds number is not fixed over a flight. As the rocket climbs, air density falls faster than speed rises, so the body-scale Reynolds number decreases with altitude even as the vehicle accelerates; it nonetheless stays far above the local transition value, $Re_x \sim 5\times10^5$, for essentially the whole atmospheric portion of the ascent. The practical conclusion, and the one this section set out to justify, is that a launching rocket's boundary layer is turbulent almost everywhere and almost always. Its friction, its boundary-layer thickness, and its resistance to separation are turbulent-flow physics from just above the launch rod to well past burnout, and the fin-level laminar patch identified in Section 3 is the exception, not the rule.

8. Closing the Loop: The Flight Experiment

Everything above is testable in a schoolyard. The protocol flies four rockets identical except for fin planform — the four rows of Table 1, all fins cut to 25 cm² from the same balsa sheet so that shape, not area, is the variable — five flights each in randomized rounds, wind capped at 3 m/s, liftoff mass equalized to ±2 g with nose ballast, motors drawn from one production lot. Apogee comes from a shared barometric altimeter (±1–3 m); launch behavior in the first 10 m is scored 1 to 3; a one-way ANOVA at $\alpha = 0.05$ with Tukey pairwise comparisons tests the planform effect [10]. A literature-derived elliptical–rectangular gap on the order of tens of meters, set against a flight-to-flight SD of 7–10 m, would give such a design real statistical power, and back-fitting an effective C_D to each measured apogee expresses the flight data in the same currency as the CFD literature. Two hypotheses do the work: H1, apogee ranks elliptical ≈ trapezoidal > clipped delta > rectangular with the extreme gap exceeding 10%; H2, the clipped delta flies straightest in calm air but weathercocks first as wind approaches 3 m/s — which is Eq. (12) read off the launch rail. If the experiment returns a null result, the protocol itself says where to look: wind variance or unequal edge finishing, both diagnosable from the logged data.

9. Conclusion

A small rocket's launch compresses a remarkable amount of physics into three seconds. The motor that lifts it is itself a Navier–Stokes flow, its thrust the momentum and pressure terms of a choked de Laval nozzle (Section 6). The flow it climbs through is incompressible Navier–Stokes at $Re \approx 2 \times 10^5$, with its pressure field fixed instant-by-instant by a Poisson equation whose source-free limit is Laplace's equation, and whose largest turbulent-regime drag term, skin friction, is exactly the viscous physics that Poisson's equation discards and Section 7's Reynolds number brings back, boundary layer, wall shear, and drag crisis included. Its trajectory follows Newton's variable-mass equation, in which a planform-driven C_D spread of 0.42–0.54 becomes a 17 m apogee spread on a B6-class motor. Its stability is a damped oscillator delivered by Lagrange's equations, stiffness proportional to static margin, safe between roughly 1 and 2 calibers and weakest just off the rod where v^2 is small. In Hamilton's variables the same dynamics become geometry — a gust lifts the vehicle onto a high energy contour and drag walks it back down, $dH/dt = -C\_\theta\theta^2$ — and in Poisson's bracket the fin set's symmetry becomes a one-line conservation law for roll. The fin that makes all this work best is a variational object: the elliptical lift distribution falls out of an Euler–Lagrange equation with a Lagrange multiplier, and the flight-validated record honors it, from the 25% drag reduction of elliptical fins to the trapezoid's repeated wins on apogee at $e \approx 0.98$ with buildable edges. The immediate next step is empirical: fly the four-planform, equal-area protocol and check whether the predicted 188–217 m ranking survives contact with real wind and real balsa. Beyond that, the natural extension is to let the constrained optimization of Section 5.3 run free — span and area as continuous variables on the stability boundary — and see whether a student-built rocket can find, by response surface and ANOVA, the same optimum the calculus of variations wrote down in 1918.

References

[1] Barrowman, J. S., and Barrowman, J. A., “The Theoretical Prediction of the Center of Pressure,” NARAM-8 R&D Report, National Association of Rocketry, 1966.

[2] Shahir, M. H., et al., “A Study on Aerodynamic Shape of Fin of Model Rocket,” Research Progress in Mechanical and Manufacturing Engineering, Vol. 2, No. 2, 2021, pp. 988–996.

[3] Pektaş, A., Ejder, E., et al., “Effects of Different Fin Shapes on Apogee and Stability of Model Rockets,” Proceedings of the IEEE International Conference on Recent Advances in Space Technologies (RAST), 2019.

[4] “Low Altitude Local Rocket Aerodynamics Analysis and Experimental Testing,” CFD and flight-test study of twelve nose-cone/fin configurations at 66 m/s, Sciforum/ASEC proceedings, 2023.

[5] “Aerodynamic Optimization and Thermal Deformation Effects on Mid-Altitude Sounding Rockets: A Computational and Structural Analysis,” OpenRocket v23.09 and SolidWorks 2024 CFD–FEA study, 2025.

[6] “Aerodynamic Study of Various Fins for Missile Body,” International Journal for Research in Applied Science and Engineering Technology (IJRASET), Vol. 11, 2023 (six planforms, Mach 0.5–2.5).

[7] “The Effect of Various Fin Designs on the Stability, Maximum Height, and Drag of Model Rockets to Maximize Efficiency,” Journal of High School Research, Vol. 2, No. 1, 2025.

[8] Van Milligan, T., “What Is the Best Fin Shape for a Model Rocket?,” Peak of Flight Newsletter, No. 442, Apogee Components, 2017.

[9] Dahlke, C. W., “The Aerodynamic Characteristics of Wrap-Around Fins at Mach Numbers of 0.3 to 3.0,” American Institute of Aeronautics and Astronautics, 1983.

[10] “The Effect of Fin Planform Geometry on the Launch Behavior and Apogee of Model Rockets: An Experimental Protocol and Expected Results,” companion experimental study, 2026.

[11] Anderson, J. D., Fundamentals of Aerodynamics, 6th ed., McGraw-Hill, 2017.

[12] Goldstein, H., Poole, C., and Safko, J., Classical Mechanics, 3rd ed., Pearson, 2002.

[13] Prandtl, L., “Über Flüssigkeitsbewegung bei sehr kleiner Reibung,” Proc. 3rd Int. Math. Congress, Heidelberg, 1904, pp. 484–491.

[14] Noether, E., “Invariante Variationsprobleme,” Nachrichten der Akademie der Wissenschaften Göttingen, 1918, pp. 235–257.

[15] Box, G. E. P., and Wilson, K. B., “On the Experimental Attainment of Optimum Conditions,” Journal of the Royal Statistical Society B, Vol. 13, 1951, pp. 1–45.

[16] Landau, L. D., and Lifshitz, E. M., Fluid Mechanics, 2nd ed., Pergamon, 1987.

[17] Schlichting, H., and Gersten, K., Boundary-Layer Theory, 9th ed., Springer, 2017.

[18] Sutton, G. P., and Biblarz, O., Rocket Propulsion Elements, 9th ed., Wiley, 2016.